



OPEN

Structural, optical, and cytotoxicity studies of laser irradiated ZnO doped borate bioactive glasses

Ahmed R. Ghazy^{1✉}, B. M. Elmowafy¹, A. M. Abdelghany², T. M. Meaz¹, R. Ghazy¹ & R. M. Ramadan³

Borate glasses (BG) doped with different amounts of ZnO (0–0.6 mol%) were formed by the traditional melt quenching technique. The different glasses so made were characterized using different characterization techniques such as X-ray diffraction (XRD), Fourier transform infrared spectroscopy (FTIR), scanning electron microscope (SEM), and UV–Vis absorption optical properties. The XRD patterns showed an amorphous structure with one broad peak at $2\theta = 29^\circ$, while the phonons bands were studied in terms of the FTIR bands. Optical properties of the glasses were studied using UV–Vis absorption spectra in the range 190–1100 nm, in which the prominent band lies at about 261.5 nm of peak position, from which the bandgap (E_g) was calculated from its edge using Tauc's plot, with $E_g \sim 3.5$ eV. The laser irradiation showed no significant changes in the absorption bands, despite a significant change observed in the amorphous behavior in the XRD pattern. The cell viability was performed for two samples of the BG and 0.6 mol% ZnO doped using 3-(4,5-dimethyl-2-thiazolyl)-2,5-diphenyl-2H-tetrazolium bromide (MTT) assay method. The result showed better cell viability and low toxicity. So, ZnO doped BG can be used in various biomedical applications.

In the last decades, the field of biomaterials has grown at an incredible rate, leading to the development of bioactive materials, which may elicit specific and predictable responses from cells and tissues¹. The discovery of Hench glass in 1969 constituted for the first time a revolution in the history of biomaterials^{2,3}. The mechanical, bioactive, and structural properties of the bioactive glasses are largely based on synthesis procedures, composition, particle size, crystallization, etc. Bioactive glasses are made using several approaches. The most common method for making bioactive glasses is the traditional melt-quenching method, in which all the components are well mixed in a ball mill before being melted at an elevated temperature⁴. In the melt-quenching process, a volatile part such as B_2O_3 gets evaporated out^{5–7}.

In constructing a bioactive glass, understanding how the physicochemical structures of these materials influence their characteristics is critical, as it allows the material to be adapted for particular applications. Each component influences the bioactive glass's performance. Calcium, for example, promotes osteoblast development and apatite layer precipitation^{8,9}. Na_2O , K_2O , MgO , CaO , P_2O_5 -based glasses found to constitute a promising material for bioactive applications such as bone repair, tissue regeneration in the human body, etc.^{10–13}. Borate glasses quickly release significant amounts of boron, leading to a high concentration of local boron near the glass. As a result, compared to silicate glasses, the degradation and sintering behavior of borate/borosilicate glass is more controllable^{14–16}. In borate glasses, the boron oxide appears in BO_3 and BO_4 in a network structure that forms 'super structural' units (pentaborate, boroxol ring, diborate, or tetraborate groups), depending on the composition and the kind of added glass modifiers^{17–20}.

The glass exhibits nonlinear change in its physical properties when one alkali ion is replaced with another alkali content at a constant amount, resulting in a mixed alkali effect (MAE)²¹. Incorporation of zinc oxide in glass structures is expected to act as an intermediate oxide either as network former or as network modifier^{22,23}. Glass composition is modified by introducing the 'dopants' to the glass network to form the desired glass where it can be bioactive, bioresorbable, and/or biodegradable. Dopants like Cu, Zn, In, Ba, La, Y, Fe, Cr, and Sr as ions lead to trigger the properties. ZnO/MgO additives have been shown to stimulate osteoblast proliferation, differentiation, and bone mineralization^{24–27}. Zn is an essential trace element that is used by various metalloenzymes for structure, catalysis, or regulatory functions. Zinc is involved in bone metabolism, enhancing osteoblastic bone

¹Physics Department, Faculty of Science, Tanta University, Tanta 31527, Egypt. ²Spectroscopy Department, Physics Research Institute, National Research Centre, 33 Elbehouth St., Dokki, Giza 12311, Egypt. ³Microwave Physics and Dielectrics, Physics Research Institute, National Research Centre, 33 Elbehouth St., Dokki, Giza 12311, Egypt. ✉email: ahmed.ghazy@science.tanta.edu.eg; aghazy57@yahoo.com

formation and preventing osteoclastic bone resorption, raising bone mass²⁸. Nutritional zinc supplementation has been demonstrated to have preventive and therapeutic effects on bone loss induced by bone disorders^{29,30}. Investigations have also demonstrated that small quantities of Zn induced early cell proliferation and enhanced differentiation of in vitro biocompatibility studies^{31–33}. Methodologies like MTT and MTS are used to assess the viability and cytotoxicity of the glass samples because these methods generally measure cytotoxicity for bulk constructions indirectly by extracting the materials.

According to Saranti et al., boron oxide has a catalytic action that promotes bioactivity³⁴. Neáková et al. developed mesoporous bioactive glass nanoparticles (MBGNs) based on the SiO₂–CaO system using a micro-emulsion supported sol–gel method. Zn²⁺ ions were doped into MBGNs with 8 Mol% ZnO concentration (Zn-MBGNs). The findings investigated that the addition of zinc precursors had no effect on particle morphology, but enhanced their specific surface area when compared to MBGNs³⁵. Lee et al. reported that bone implant and osteointegration utilizing a B₂O₃-based glass technology represents no toxicity. Bone implant and osteointegration using B₂O₃ based glass system are reported by Lee et al. without any toxicity³⁶. Kolavekar et al. studied the optical properties of Pr₂O₃-doped multi-component borate glasses³⁷, TeO₂-doped lead borate glasses³⁸, Li⁺ ions doped zinc borate glass³⁹ and Er³⁺ and Er³⁺/Yb³⁺ co-doped heavy metal borate glasses⁴⁰ and showed the effect of the dopants on the photophysical properties of the borate glass.

Bioactive glasses are effective biomaterials for promoting angiogenesis in both hard and soft tissue engineering applications. Metallic ions like Cu²⁺, Ag²⁺, Mg²⁺, Zn²⁺, Fe³⁺, Sr²⁺, and Co²⁺ have been utilized as dopants in oxide glasses^{41–43}. The presence of these ions in the glass network causes antibacterial agents, osteogenesis motivation factors, and angiogenesis enhancers^{44,45}.

The effect of laser irradiation was studied for borosilicate glasses attracted much of scientists attention because it can stimulate various microspheres that can be controlled within transparent materials due to non-linear optical absorption^{46,47}. The novelty in the work is to study the effect of laser irradiation on the structure and optical properties of ZnO doped borate bioactive glass.

This study is aimed to investigate the effect of ZnO on the structure of bioactive borate glass using X-ray diffraction (XRD) and Fourier transform infrared spectroscopy (FTIR). The effects of laser irradiation on the selected glasses are studied in terms of their UV–Vis absorption spectra and XRD pattern. The cytotoxicity of ZnO-doped bioactive borate glass on cell viability is assessed in a contest to bioapplications.

Experimental work

Materials(glasspreparation). The glasses of compositions 6Na₂O + 12K₂O + 5MgO + 20CaO + 4P₂O₅ + (53-x) B₂O₃ + xZnO (0 ≤ x ≤ 0.6 mol%), were prepared via traditional melt quenching method. Highly pure chemicals of orthoboric acid (a source for B₂O₃) and ammonium dihydrogen phosphate (a source for P₂O₅) supplied by Sigma Aldrich Co were used. Na₂O, K₂O, MgO, and CaO were added as carbonates provided by El Nasr Pharmaceuticals. All the chemicals were used as received. The chosen glass batches were mixed and melted in an electrical furnace at 1100–1150 °C and swirled to assure homogeneity, and then the melts were quenched and pressed between two steel plates at room temperature to obtain the glasses. The so-obtained glasses were characterized using XRD patterns, FTIR, and UV–visible absorption spectra. Images of the formed glasses are listed in the Table 1.

Characterization and analysis techniques. The various methods of analysis and typical settings that describe ZnO doped borate glass are recorded by utilizing the following instruments: (a) the X-ray diffraction pattern (XRD) was recorded in the range of 4° ≤ 2θ ≤ 70° using a Rigaku X-ray diffractometer ultima IV with CuKα radiation of wavelength λ = 0.154600 nm and steps of 0.02°. (b) Microstructure of the samples was examined using a scanning electron microscope (JEOL JSM-6510LV, USA), which used a focused electron beam (operating at 20 kV accelerating voltage) with a magnification up to 40,000 X, where the samples were coated with gold so the surface becomes conducting to measure the images. (c) A FTIR spectrometer (type Nicolet i10, Thermo Fisher Co.) was used to record FTIR spectra of the glasses over a 4000–400 cm⁻¹ range, with a 2 cm⁻¹ step resolution. Measurements were performed on powders dispersed in KBr in a 1:100 ratio in the form of thin pellets. (d) UV/Visible absorption spectra were recorded (in a range of 190 to 1100 nm) for the polished samples, using a double beam (JASCO V570 UV/Vis./NIR) spectrophotometer, with air as a reference sample. All the glass samples were irradiated for 30 min by a laser beam (λ = 375 nm) with a 150 mV power.

The technique of 3-(4,5-dimethyl-2-thiazolyl)-2,5-diphenyl-2H-tetrazolium bromide (MTT) assay technique was used to assess cytotoxicity and proliferation was purchased from (Serva, Germany). Cells were seeded in well plates and cultured for 48 h to determine the IC₅₀ for the different glasses and compared with the control sample (normal cell without glass). The glass was solubilized in dimethyl sulfoxide (DMSO) stock before treatment.

Sample	Base	0.1 mol% ZnO	0.2 mol% ZnO	0.3 mol% ZnO	0.4 mol% ZnO	0.6 mol% ZnO
Image						

Table 1. Photo images of borate glass doped with different amounts of ZnO.

The reduction in cell growth was measured at (570 nm) (BioTek, Elx800, US) and the results were calculated as a percentage of control. Prism software was used to calculate the IC50 of glass concentrations as well as cell viability.

Results and discussion

XRD patterns and microstructure. Figure 1 presents XRD patterns of the ZnO doped borate glass, which reveal an amorphous structure for all the samples with a broad diffraction peak at $2\theta = 29^\circ$ of diffraction angle ' 2θ ', with no sharp peak in absence of any crystallites. The absence of clearly defined diffraction peaks confirms the samples' glassy nature and rules out the possibility of long-range atomic organization^{48,49}. The absence of Bragg's peak and the amorphous glassy nature of all the glass samples were confirmed by X-ray diffraction patterns due to the presence of potassium and magnesium, in particular, which enhanced glass processability, making it easier to make glass without crystallization and use it in coatings, fibers, scaffolding and other applications⁵⁰.

Figure 2a, b represent SEM of borate glass doped with 0.6 mol% ZnO of lower and higher magnification which showed dispersed particles or grain-like structure appeared in the morphology of 0.6Mol% ZnO doped borate glass. SEM images indicate the domination of the amorphous structure of the borate matrix as a continuous phase. A good agreement with the suggested amorphous structure from the XRD pattern was demonstrated from the SEM images.

Figure 3 shows FTIR spectra of the ZnO doped borate glass where there were broad absorption bands that indicate the groups inside the network system. The interpretation of IR of borate glass is summarized as follows: The first broad band around 1396 cm^{-1} indicated for B–O asymmetric stretching vibration band of trigonal BO_3 . The second band at 1008 cm^{-1} pointed to the B–O bond stretching of the tetrahedral BO_4 . The third band positioned nearly at 714 cm^{-1} refers to the bending of B–O–B in trigonal BO_3 units and the last band at 563 cm^{-1} points to the vibration of metal cations like ZnO. The bands face no changes when ZnO nanoparticles are added to the composition. The strong appearance of vibrational broad bands of triangular and tetrahedral for borate glass owing to the presence of the two alkali metals Na_2O and K_2O . Also, many little changes were investigated after the minor addition of ZnO nanoparticles which indicated the effect of the concentration of ZnO nanoparticles on the transformation process. The band appears in the far infrared region 425 cm^{-1} due to

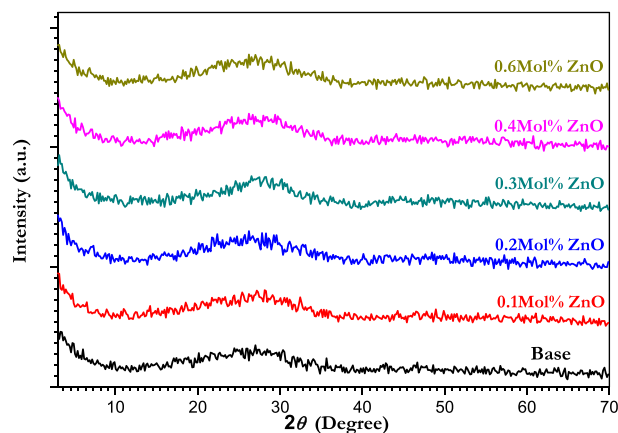


Figure 1. XRD patterns of different concentrations of ZnO doped borate glass in the range of $4^\circ \leq 2\theta \leq 70^\circ$.

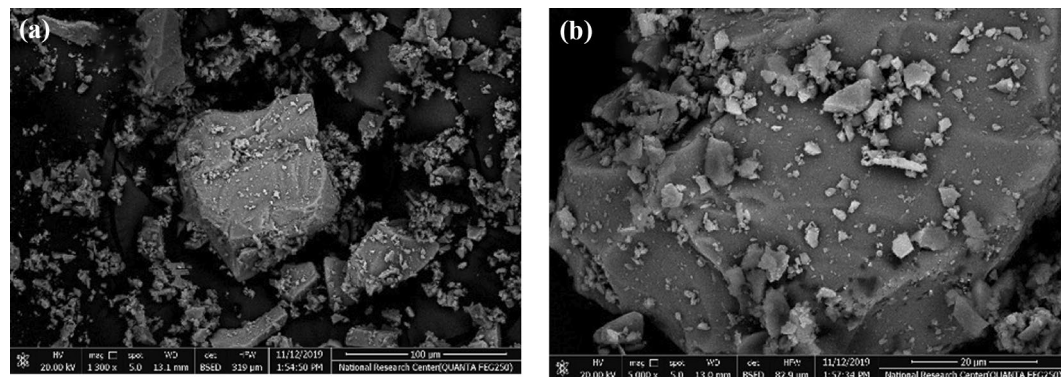


Figure 2. SEM images of borate glass doped with 0.6 mol% ZnO; (a) lower (b) higher magnifications.

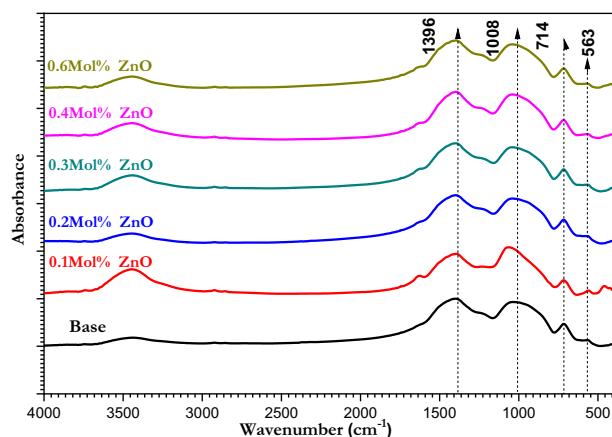


Figure 3. FTIR spectra of borate glasses doped with different concentrations of ZnO.

the stretching vibration of transition metal ions such as (Zn^{2+} , and Mn^{2+}). The other main vibrational modes mentioned before are due to the borate glass matrix⁵¹.

PeakFit4.12 computer program was used for the mathematical deconvoluted analysis technique (DAT) that was used to examine and analyze the collected FTIR spectral data of ZnO-doped borate glasses to obtain quantitative information about the internal changes inside the glass matrix. In the range of 1750–500 cm^{-1} , the smeared overlapping bands of triangular and tetrahedral borate groups were resolved, while the region of 3200–3600 cm^{-1} reveals the vibrational modes of the OH group. The deconvoluted analysis was established using a small number of bands to resolve the spectra and then weaker bands were inserted to improve the fit. Figure 4a–e represents the deconvoluted analysis of ZnO-doped borate glasses and their residuals. The deconvolution process is based on the previous knowledge of the wavenumber of suggested vibrational groups and the second derivative of the spectrum that identifies the accurate position of peak maxima as previously described by different authors^{52–56}. In such cases, the differences between the deconvoluted and measured spectrum can be minimized and plotted as shown in the residual curves.

Obtained N4 data of coordinated boron ($N4 = \text{BO}_4 / (\text{BO}_4 + \text{BO}_3)$) for ZnO doped borate glasses is represented in Fig. 5, which indicates boron atoms transformations occur inside the glass matrix after ZnO nanoparticles addition. It can be figured that the value of N4 increased by increasing the concentration of ZnO nanoparticles to 0.2 mol% and then faces two stages of decreasing and increasing. The creation of non-bridging oxygen NBOs can be correlated with the decrease in the N4 ratio with increasing in ZnO nanoparticles content in addition to other parameters. The negative charge on NBOs makes it easier for electrons to be excited at higher wavelengths⁵⁷. Both ZnO and CaO act to reduce the $\text{BO}_4 / (\text{BO}_4 + \text{BO}_3)$ ratio and enhanced the glass network by increasing the number of non-bridging oxygen atoms⁵⁸. In the glass structure, ZnO acts as an intermediate oxide either as network former or as network modifier⁵⁹, where ZnO nanoparticles is a promising candidate as a modifier with a large band gap, allowing it to be used as a potential optical material^{48,60}. As there was an unnoticeable change ZnO nanoparticles act as a modifier not as a former.

Electronic absorption spectra. Ultraviolet–visible absorption spectroscopy represents the optical properties that give information about the electronic structure of the material^{61,62}. UV–Vis. absorption spectra of ZnO doped borate glasses were explained in Fig. 6 in the wavelength range of 190–1100 nm. It can be figured that the absorption of UV–Vis arises from the higher wavelength to the lower wavelength of the glass materials. A high absorption band at the wavelength of 261.75 nm in the UV region of the spectrum was figured out for all doped glasses, which results from the unavoidable trace iron impurities in the raw materials during the glass formation⁶³. While the broad absorption band between 200 and 340 nm is due to high valence or tetrahedral coordination of the transition metal ions in the alkali borate glass which agreed with the data reported in^{64,65}. The nonlinear behavior of the position of the edge at around 340 nm was found to be compatible with the N4 values represented in Fig. 5. The UV absorption of glasses is considered to be influenced by both internal and external factors such as the electronic transitions, which are primarily caused by the addition of dopants and are influenced by the glass structure and chemical bonding⁶⁶. Also, the change in the position of the absorption edge is due to the variation of oxygen bonding in the glass network⁶⁷. The addition of metal cations such as Pb, Zn, Cd, and others affects the network formation of B_2O_3 and SiO_4 . These additives also act as a network modifier and a nucleating agent for glass crystallization. As a result, the optical properties of borate glasses have changed significantly⁶⁸.

Using a diode laser with a wavelength of 375 nm and 150 mW power the ZnO-doped borate glasses were irradiated for 30 min at room temperature. Figure 7a–f represents the absorption spectra for ZnO-doped borate glasses before and after the irradiation process. It can be figured that there was an absorption band in the UV region and no visible bands were observed for ZnO-doped borate glasses before and after the irradiation process as can be seen in Fig. 7a–f, only a change in the absorption intensity for the absorption band in the UV region

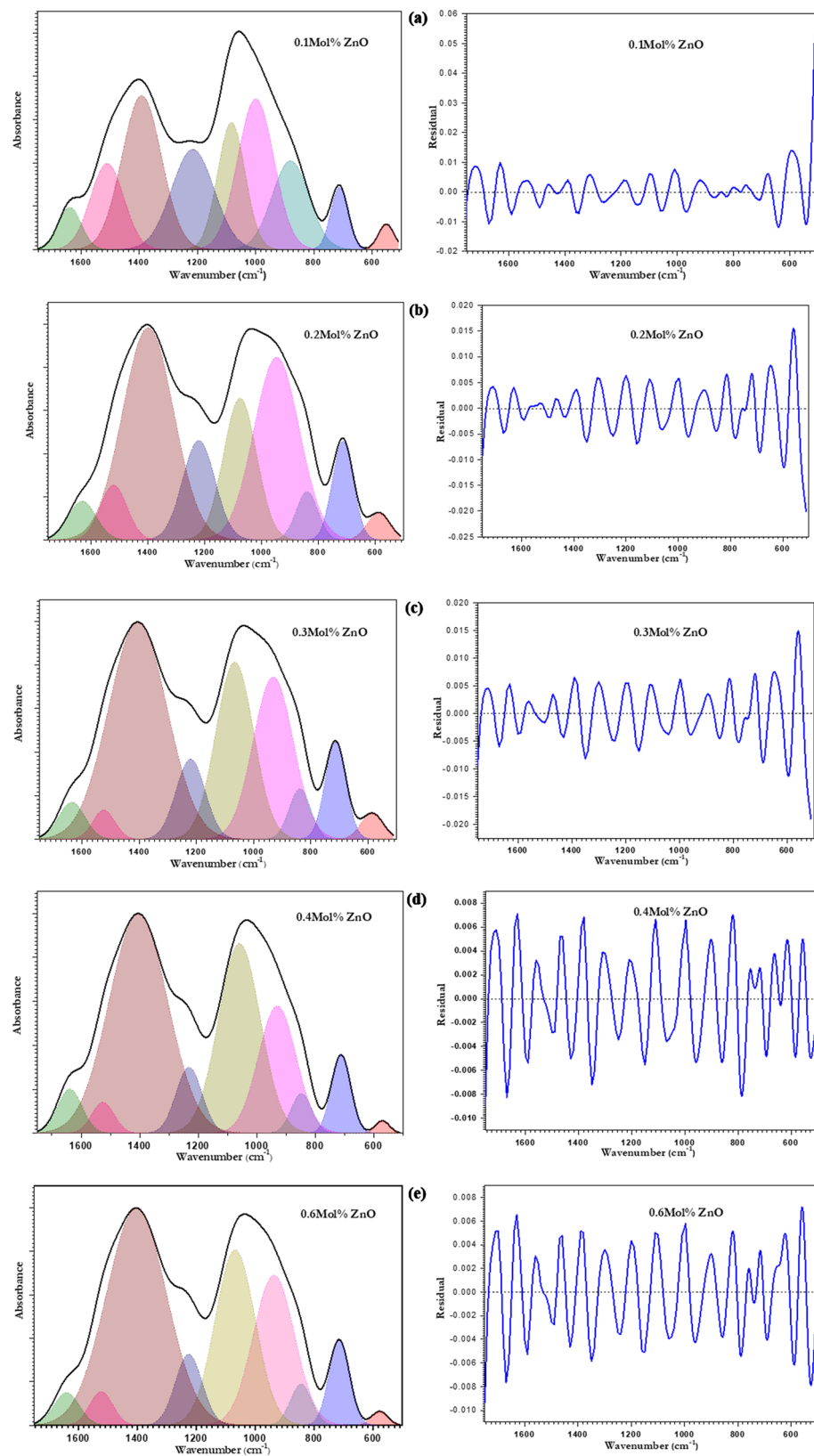


Figure 4. The deconvolution of FTIR spectra with its residual of ZnO doped borate glasses.

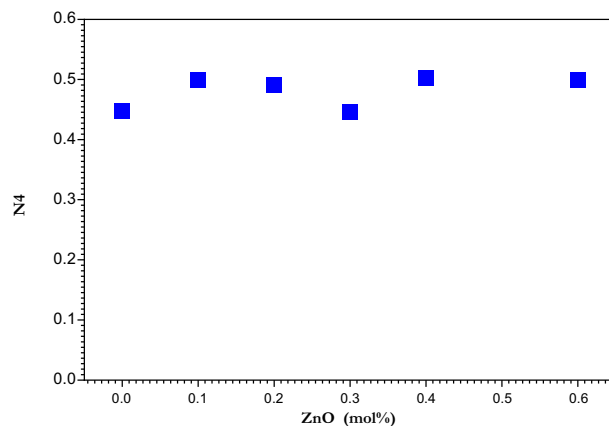


Figure 5. Variation of the fraction of four coordinated boron as a function of ZnO nanoparticles concentration.

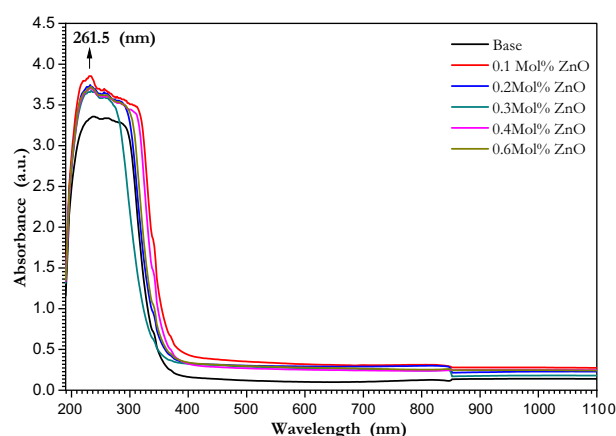


Figure 6. Absorption Spectra of ZnO doped borate glasses in the range of 190–1100 nm.

and a small shift to the edge wavelength λ_{edge} were observed. The values of the λ_{edge} and direct optical energy gaps were calculated using Tauc plots and the Mott-Davis model $(\alpha h\nu)^2 = B(h\nu - E_g)^{69,70}$ are listed in Table 2.

XRD was performed for 0.1 mol% ZnO doped sample and it's obvious that clearly defined diffraction peaks were absent confirming the samples' glassy nature and ruling out the possibility of long-range atomic organization⁴⁸. Figure 8 showed that before and after laser irradiation as there were two broad humps after laser irradiation around 29° and 46° were detected such humps distinguish non-crystalline solids (amorphous solids). Therefore, it can be stated that all studied samples are short-range order solids (glass solids).

Cytotoxicity assay. It is necessary to evaluate the cytotoxicity of the material used in bio-applications. The culture of normal human skin fibroblasts (HSF) was used and investigated the influence of the glass with different concentrations on these cells.

Glass efficiency and potency in cells exposed to a drug (glass) are commonly evaluated using drug (glass) dose–response assays (e.g. MTT assay), and then the IC₅₀ (half maximum inhibitory concentration) is estimated. With cell-based cytotoxicity studies, the 50 percent inhibitory concentration (IC₅₀) is commonly employed to measure drug potency⁷¹. Zinc ions have also been linked to a variety of physiological activities, such as cell proliferation⁷². The result of cell viability was determined for the undoped and 0.6 mol% ZnO doped borate glasses Table 3. From the data in the table starting from 50 to 1.5625 μM of the glass material where a low concentration of each glass (1.5625 μM) gives a high percentage of viable cells, and also, they are non-toxic. After increasing the concentration of the glass material, the values of cell viability are still good compared to cell viability values in^{73,74}.

Figure 9a,b represent the dose–response curves cytotoxicity assay of the undoped and 0.6 mol% ZnO doped borate glasses with different concentrations incubated in cell culture and showed the half-maximal inhibitory concentration (IC₅₀). The standard error of the mean is represented by the error bars. Prasad S⁷⁵, investigated in vitro cell proliferation using the MTT test on the base glass (BG0B) selected from the SiO₂–Na₂O–CaO–P₂O₅ system (S53P4 glass), as well as various modified glass compositions generated by replacing SiO₂ in the base glass composition by B₂O₃ (BG1B, BG2B, and BG3B). It demonstrates that the cell proliferation was better on the

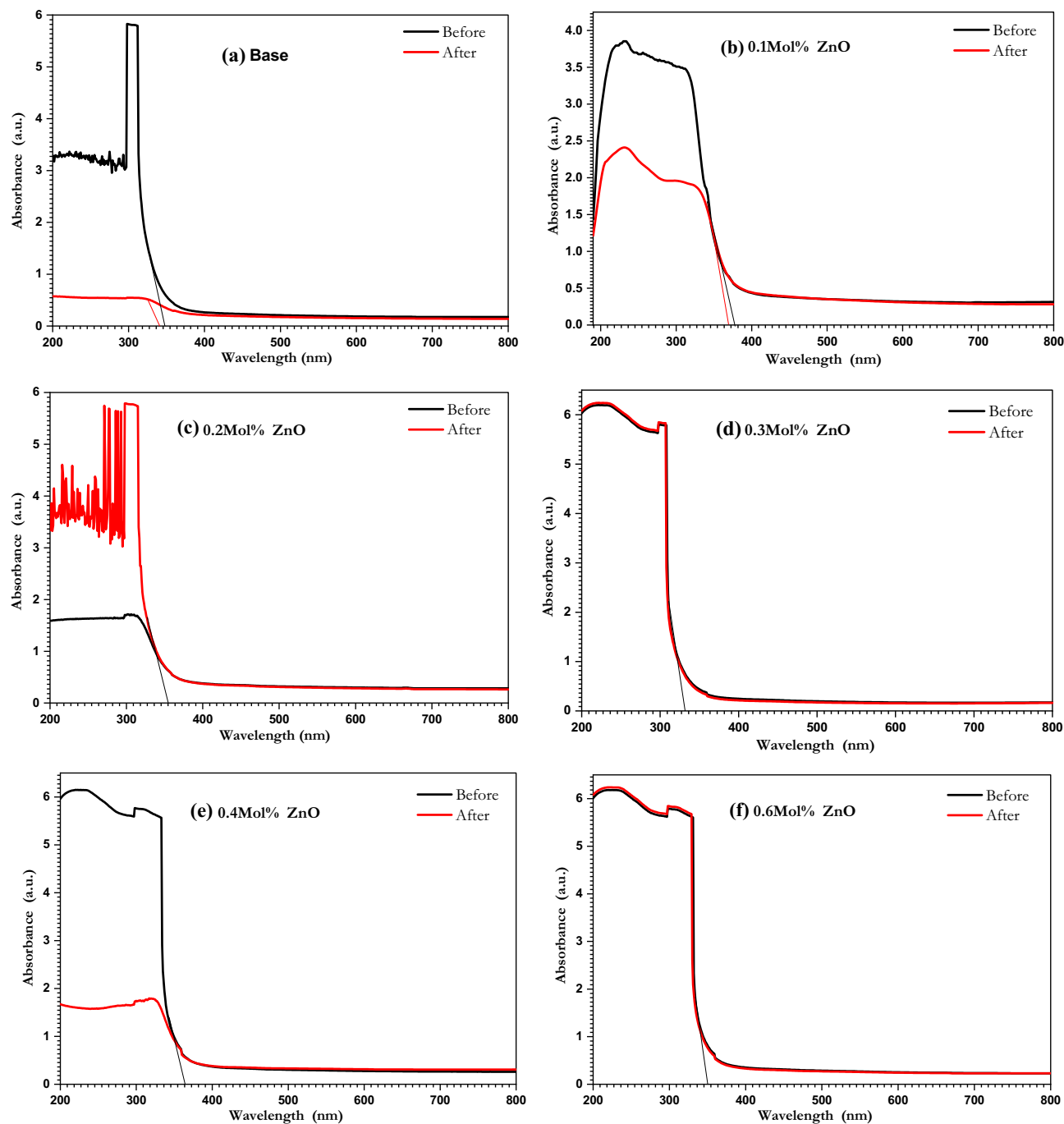


Figure 7. UV-vis absorption spectra of ZnO doped borate glasses before and after 30 min of laser irradiation.

Sample	Before		After	
	$\lambda_{\text{edge}}(\text{nm})$	$E_g^{\text{opt}}(\text{eV})$	$\lambda_{\text{edge}}(\text{nm})$	$E_g^{\text{opt}}(\text{eV})$
Base	348.03	3.56	338.73	3.66
0.1 mol% ZnO	367.3	3.38	378.29	3.28
0.2 mol% ZnO	354.81	3.49	354.81	3.49
0.3 mol% ZnO	334.08	3.71	334.08	3.71
0.4 mol% ZnO	364.11	3.41	364.11	3.41
0.6 mol% ZnO	350.36	3.54	350.36	3.54

Table 2. Optical energy gap before and after laser irradiation for ZnO doped borate glasses.

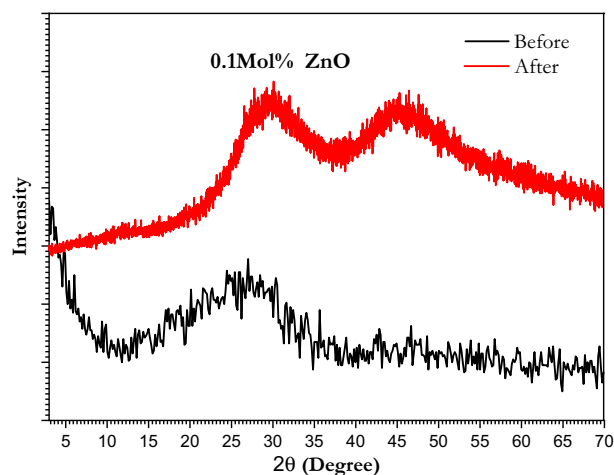


Figure 8. X-ray diffraction pattern of borate glass doped with 0.1 mol% ZnO before and after 30 min of laser irradiation.

Glass	Cell viability %					
	50	25	12.5	6.25	3.125	1.5625
Base	89.28877	95.11568	96.11568	98.9709	101.1705	102.6281
	88.94773	94.14567	95.74464	97.34362	100.3436	103.1722
0.6 mol% ZnO	74.72151	82.26221	87.97601	90.48843	93.91602	95.45844
	83.69494	87.89289	91.52014	97.8329	99.11911	101.8029

Table 3. Values of cell viability of the undoped and 0.6 mol% ZnO doped borate glasses with different concentrations of each glass.

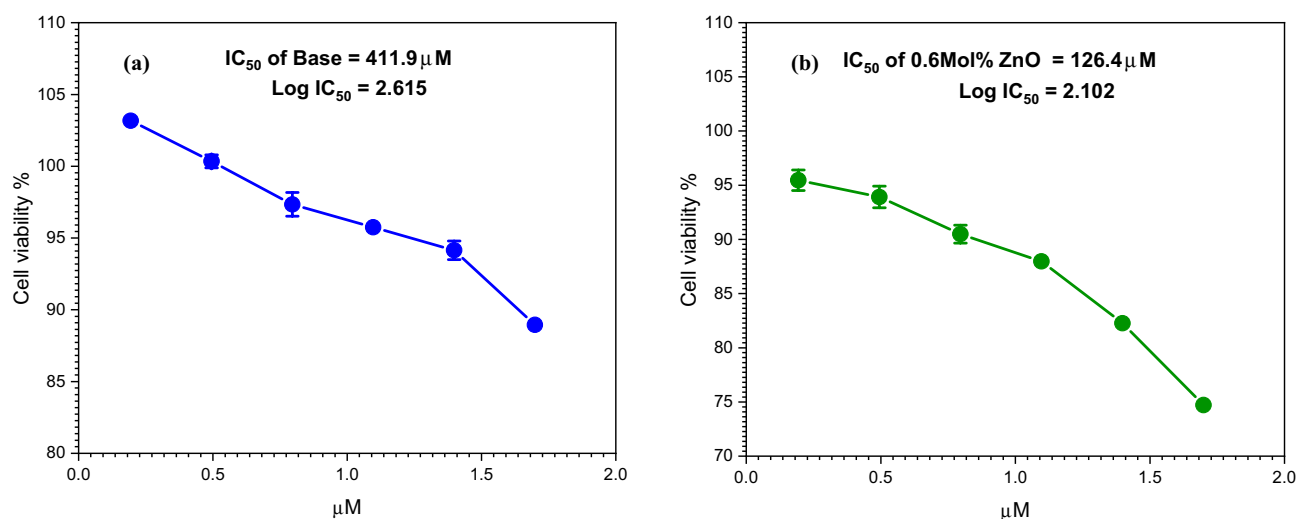


Figure 9. Effect of different amounts of (a) undoped glass, (b) 0.6 mol% ZnO doped borate glass on cell viability assay as determined from the absorbance at 570 nm and corresponding IC₅₀ values.

B₂O₃-modified glasses (BG1B, BG2B, and BG3B) compared to the base glass (BG0B). It's founded that cell growth was better on the B₂O₃-modified glasses (BG1B, BG2B, and BG3B) when compared to the base glass (BG0B). According to Balasubramanian et al.⁷⁶ adding boron to bioactive glasses in various quantities has substantial effects on glass structure, glass processing characteristics, biodegradability, biocompatibility, bioactivity, and cytotoxicity. For bone and soft tissue engineering, various compositions of boron-doped, borosilicate, and borate glasses, are being studied. After cytotoxicity tests, the optical microscope image of the cells was taken (Fig. 10a–c). The morphology of cells that extend over the dish surface was not changed in the samples that showed low

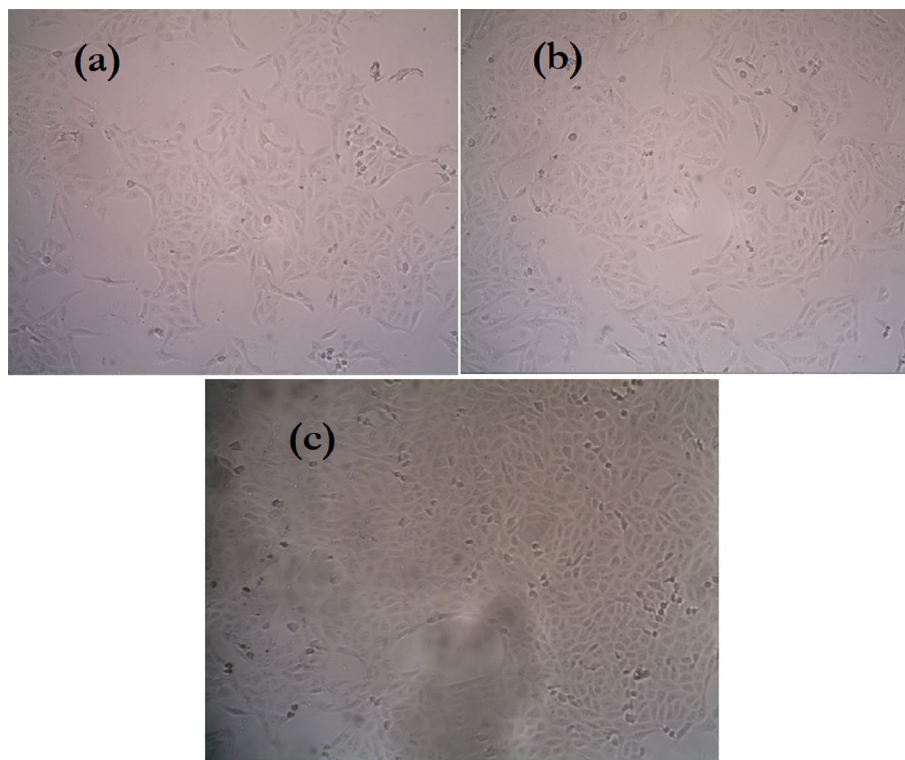


Figure 10. The optical microscope image of (a) undoped glass, (b) 0.6 mol% ZnO doped borate glass after cytotoxicity tests compared to (c) control sample.

cytotoxicity as compared to the control sample. The morphology of the cells was approximately similar compared to the control sample, where the pulp cells indicated the survival cells and the rounded or shrunk cells indicated dead cells. It's concluded that non-toxic behavior is exhibited by the prepared glasses compared to the control sample cells. Also, it is appropriate to be used for human tissue with no harmful effects.

Conclusions

In this study, ZnO doped borate glasses with a composition of $6\text{Na}_2\text{O} + 12\text{K}_2\text{O} + 5\text{MgO} + 20\text{CaO} + 4\text{P}_2\text{O}_5 + (53-x)\text{B}_2\text{O}_3 + x\text{ZnO}$, ($0 \leq x \leq 0.6$ mol%) were synthesized by traditional melt quenching technique. XRD study showed a high degree of amorphous structure for all samples. The formation of borate glass and the interaction with ZnO nanoparticles were indicated successfully by FTIR spectroscopy. Deconvolution analyses were applied to analyze the collected FTIR spectral data and showed a slight change in N4 coordinated boron but wasn't noticeable due to the minor addition of zinc oxide. The incorporation of TMI was found to produce BO_3 and BO_4 structural units by shattering the boroxol (B_3O_6) ring, according to Fourier transform infrared (FTIR) spectra. UV-Vis optical properties were applied, and the optical energy gap was found to be around 3.4 eV. A highly intense band in the UV region in the range between 200 and 270 nm was noticed and found to be due to unavoidable trace elements introduced by raw materials. After the laser irradiation process, the optical energy gap was nearly similar for all samples but there was a change in the absorption intensity. The XRD pattern showed a change in the structure after the irradiation process, which indicate the short-range order of the investigated glass. Good cell viability was found for 0.6 mol% ZnO doped borate glass compared to the undoped glass after using the MTT assay method, the value of IC_{50} was decreased from 411.9 μM for borate glass to 126.4 μM for 0.6 mol% ZnO doped borate glass. As a result of that, and after future study on biodegradation and activity, ZnO-doped borate glasses with nominal composition is recommended for in vitro and in vivo bio applications.

Data availability

No data was used for the research described in the article. The data presented in this study are available in the article.

Received: 15 March 2023; Accepted: 30 April 2023

Published online: 05 May 2023

References

1. Marchi, J. *Biocompatible Glasses: From Bone Regeneration to Cancer Treatment* (Springer, 2016).
2. Hench, L. L. The story of bioglass*. *J. Mater. Sci. Mater. Med.* **17**, 967–978 (2006).
3. Lung, C. Y. *et al.* A multi-element-doped porous bioactive glass coating for implant applications. *Materials* **14**, 961 (2021).

4. Ram, S., Chakravorty, D. & Bahadur, D. Effect of nucleating agents on the crystallisation behaviour of barium hexaferrite in a borate glass. *J. Magn. Magn. Mater.* **62**, 221–232 (1986).
5. Kaur, G. *et al.* Synthesis, cytotoxicity and hydroxyapatite formation in 27-Tris-SBF for sol-gel based CaO-P₂O₅-SiO₂-B₂O₃-ZnO bioactive glasses. *Sci. Rep.* **4**, 1–14 (2014).
6. Mehrabi, T. & Mesgar, A. S. In vitro biomineralization potential in simulated wound fluid and antibacterial efficacy of biologically-active glass nanoparticles containing B₂O₃/ZnO. *Colloids Surf., B* **212**, 112338 (2022).
7. Elmowafy, B. M., Abdelghany, A., Ramadan, R. M., Ghazy, R. & Meaz, T. Synthesis, structural characterization, and antibacterial studies of new borate 13–93B3 bioglasses with low copper dopant. *Egypt. J. Chem.* **65**, 1–2 (2022).
8. Maeno, S. *et al.* The effect of calcium ion concentration on osteoblast viability, proliferation and differentiation in monolayer and 3D culture. *Biomaterials* **26**, 4847–4855 (2005).
9. Wang, C., Meng, C., Zhang, Z. & Zhu, Q. 3D printing of polycaprolactone/bioactive glass composite scaffolds for in situ bone repair. *Ceram. Int.* **48**, 7491–7499 (2022).
10. Kokubo, T. & Takadama, H. How useful is SBF in predicting in vivo bone bioactivity?. *Biomaterials* **27**, 2907–2915 (2006).
11. Zhu, H. *et al.* 3D bioprinting of multifunctional dynamic nanocomposite bioinks incorporating Cu-doped mesoporous bioactive glass nanoparticles for bone tissue engineering. *Small* **18**, 2104996 (2022).
12. Al-Harbi, N. *et al.* Silica-based bioactive glasses and their applications in hard tissue regeneration: A review. *Pharmaceuticals* **14**, 75 (2021).
13. Kiran, P., Ramakrishna, V., Trebbin, M., Udayashankar, N. & Shashikala, H. Effective role of CaO/P₂O₅ ratio on SiO₂-CaO-P₂O₅ glass system. *J. Adv. Res.* **8**, 279–288 (2017).
14. Zhang, X. *et al.* Teicoplanin-loaded borate bioactive glass implants for treating chronic bone infection in a rabbit tibia osteomyelitis model. *Biomaterials* **31**, 5865–5874 (2010).
15. Gupta, S., Majumdar, S. & Krishnamurthy, S. Bioactive glass: A multifunctional delivery system. *J. Control. Release* **335**, 481–497 (2021).
16. Henaish, A. *et al.* A comparative study of optical vanadium antimony borate glass doped with spinel ferrite using structural, spectral, and electrical measurements. *Appl. Phys. A* **128**, 1–19 (2022).
17. Yano, T., Kunimine, N., Shibata, S. & Yamane, M. Structural investigation of sodium borate glasses and melts by Raman spectroscopy: I. Quantitative evaluation of structural units. *J. Non-Cryst. Solids* **321**, 137–146 (2003).
18. Zakaly, H. M. *et al.* An experimental evaluation of CdO/PbO-B₂O₃ glasses containing neodymium oxide: Structure, electrical conductivity, and gamma-ray resistance. *Mater. Res. Bull.* **151**, 111828 (2022).
19. Doweidar, H. & Saddeek, Y. B. FTIR and ultrasonic investigations on modified bismuth borate glasses. *J. Non-Cryst. Solids* **355**, 348–354 (2009).
20. Ram, S. & Haldar, S. Medium-range structural ordering and macroscopic interactions in 1 to 2 mm thin two-dimensional platelets of borate glasses. *Phys. Status Solidi (b)* **195**, 343–351 (1996).
21. Shan, Z. *et al.* Mixed alkaline earth effects on crystallization behavior of basalt glasses and liquids. *J. Alloy. Compd.* **874**, 159986 (2021).
22. Subhashini, Bhattacharya, S., Shashikala, H. & Udayashankar, N. Synthesis and studies on microhardness of alkali zinc borate glasses. *AIP Conf. Proc.* **1591**, 749–750 (2014).
23. Afrizal, N. H., Yahya, N., Yusoff, N. M., Kasim, A. & Hashim, A. Physical, mechanical and structural properties of yttrium oxide doped zinc borate glasses. *Solid State Phenom.* **307**, 327–335 (2020).
24. Kaur, G. *Clinical Applications of Biomaterials: State-of-the-Art Progress, Trends, and Novel Approaches* (Springer, 2017).
25. Ram, S. & Narayan, K. A. Controlled crystallization of lead oxide-chromium oxide-boron oxide (PbO-Cr₂O₃-B₂O₃) glasses and a catalytic effect of alumina for the growth of lead chromate (Pb₂CrO₅) microcrystals. *Ind. Eng. Chem. Res.* **26**, 1051–1055 (1987).
26. Ram, S., Bahadur, D. & Chakravorty, D. Magnetic and microstructural studies of Ca-hexaferrite based glass-ceramics. *J. Non-Cryst. Solids* **101**, 227–242 (1988).
27. Kumari, K., Ram, S. & Kotnala, R. Self-controlled growth of Fe₃BO₆ crystallites in shape of nanorods from iron-borate glass of small templates. *Mater. Chem. Phys.* **129**, 1020–1026 (2011).
28. Ghazy, A. R., Al-Hossainy, A. F., El-Sheekh, M. M. & Makhlof, M. E. M. Investigating the differences in structure, morphology, optical properties, laser photoluminescence and dielectric properties for chitosan-doped commercial and Polycladia myrica mediated ZnO nanoparticles films combined with TD-DFT simulations. *Algal Res.* **71**, 103076 (2023).
29. Yamaguchi, M. Role of nutritional zinc in the prevention of osteoporosis. *Mol. Cell. Biochem.* **338**, 241–254 (2010).
30. Li, H. *et al.* The role of zinc in bone mesenchymal stem cell differentiation. *Cell. Reprogram.* **24**, 80–94 (2022).
31. Balamurugan, A. *et al.* Development and in vitro characterization of sol-gel derived CaO-P₂O₅-SiO₂-ZnO bioglass. *Acta Biomater.* **3**, 255–262 (2007).
32. Naresh, P. *et al.* Preparation and Characterization of melt derived CaO-Sb₂O₃-Li₂O containing borate glass for multiple application. *J. Non-Cryst. Solids* **589**, 121642 (2022).
33. Oki, A., Parveen, B., Hossain, S., Adeniji, S. & Donahue, H. Preparation and in vitro bioactivity of zinc containing sol-gel-derived bioglass materials. *J. Biomed. Mater. Res. Part A* **69**, 216–221 (2004).
34. Saranti, A., Koutselas, I. & Karakassides, M. Bioactive glasses in the system CaO-B₂O₃-P₂O₅: Preparation, structural study and in vitro evaluation. *J. Non-Cryst. Solids* **352**, 390–398 (2006).
35. Neščáková, Z. *et al.* Multifunctional zinc ion doped sol-gel derived mesoporous bioactive glass nanoparticles for biomedical applications. *Bioact. Mater.* **4**, 312–321 (2019).
36. Lee, J. H. *et al.* In vivo study of novel biodegradable and osteoconductive CaO-SiO₂-B₂O₃ glass-ceramics. *J. Biomed. Mater. Res. Part A* **77**, 362–369 (2006).
37. Kolavekar, S. B. & Ayachit, N. Impact of Pr₂O₃ on the physical and optical properties of multi-component borate glasses. *Mater. Chem. Phys.* **257**, 123796 (2021).
38. Kolavekar, S. B. & Ayachit, N. Impact of variation of TeO₂ on the thermal properties of lead borate glasses doped with Pr₂O₃. *Eur. Phys. J. Plus* **137**, 1–8 (2022).
39. Kolavekar, S. B. & Ayachit, N. Ionic conductivity and dielectric relaxations in Li⁺ ions doped zinc borate glass system. *ECS J. Solid State Sci. Technol.* **11**, 103009 (2022).
40. Hegde, V. *et al.* Analysis of optical and near-infrared luminescence of Er³⁺ and Er³⁺/Yb³⁺ Co-doped heavy metal borate glasses for optical amplifier applications. *Photonics* **9**, 355 (2022).
41. Ram, S. & Ram, K. IR and Raman studies and effect of γ radiation on crystallization of some lead borate glasses containing Al₂O₃. *J. Mater. Sci.* **23**, 4541–4546 (1988).
42. Ram, S. Infrared study of the dynamics of boroxol rings in the crystallization of BaFe₁₂O₁₉ microcrystals in borate glasses. *Phys. Rev. B* **51**, 6280 (1995).
43. Ram, S. & Ram, K. Infrared reflectance spectra and formalism of precipitation of acicular magnetic particles in network glasses. *Infrared Phys. Technol.* **37**, 457–469 (1996).
44. Kargozar, S., Baino, F., Hamzehlou, S., Hill, R. G. & Mozafari, M. Bioactive glasses: SPROUTING angiogenesis in tissue engineering. *Trends Biotechnol.* **36**, 430–444 (2018).
45. Abouelnaga, A. M., Meaz, T. M., Othman, A. M., Ghazy, R. A. & El Nahrawy, A. M. Probing the structural and antimicrobial study on a sol-gel derived velosef-loaded bioactive calcium magnesio-silicate xerogel. *SILICON* **13**, 623–631 (2021).

46. Tostanoski, N. J., Youngman, R. E. & Sundaram, S. Effect of femtosecond laser irradiation on structure-terahertz property relationship in sodium borosilicate glasses. *Int. J. Appl. Glass Sci.* <https://doi.org/10.1111/ijag.16634> (2023).
47. Tomita, K., Kishi, T., Matsumura, D. & Yano, T. Laser heating induced spatial homogenization of phase separated Na₂O-B₂O₃-SiO₂ glass plate with bearing NiO for heat center and structural probe. *J. Non-Cryst. Solids* **597**, 121891 (2022).
48. Samir, A., Hassan, M. A., Abokhadra, A., Soliman, L. & Elokr, M. Characterization of borate glasses doped with copper oxide for optical application. *Opt. Quant. Electron.* **51**, 1–13 (2019).
49. Issever, U., Kilic, G. & Ilik, E. The Impact of CuO on physical, structural, optical and thermal properties of dark VPB semiconducting glasses. *Opt. Mater.* **116**, 111084 (2021).
50. Okumura, M. *et al.* Osteoblastic phenotype expression on the surface of hydroxyapatite ceramics. *J. Biomed. Mater. Res.* **37**, 122–129 (1997).
51. Pal, M., Roy, B. & Pal, M. Structural characterization of borate glasses containing zinc and manganese oxides. *J. Modern Phys.* <https://doi.org/10.4236/jmp.2011.29129> (2011).
52. Abdelghany, A. The elusory role of low level doping transition metals in lead silicate glasses. *SILICON* **2**, 179–184 (2010).
53. Abdelghany, A. Novel method for early investigation of bioactivity in different borate bio-glasses. *Spectrochim. Acta Part A Mol. Biomol. Spectrosc.* **100**, 120–126 (2013).
54. Abdelghany, A., Diab, H., Madbouly, A. & Ezz-ELDin, F. Inspection of radiation shielding proficiency and effect of gamma-ray on ESR and thermal characteristics of copper oxide modified borate bioglasses. *J. Inorg. Organomet. Polym. Mater.* **32**, 3204–3219 (2022).
55. Kamitsos, E. Infrared studies of borate glasses. *Phys. Chem. Glasses* **44**, 79–87 (2003).
56. Lin, Y.-T. *et al.* Photothermal atomic force microscopy coupled with infrared spectroscopy (AFM-IR) analysis of high extinction coefficient materials: A case study with silica and silicate glasses. *Anal. Chem.* **94**, 5231–5239 (2022).
57. Chanshetti, U. B., Sudarsan, V., Jogad, M. S. & Chondhekar, T. K. Effect of CuO addition on the optical and electrical properties of sodium zinc borophosphate glasses. *Physica B* **406**, 2904–2907 (2011).
58. Boda, R., Srinivas, G., Komaraiah, D., Shareefuddin, M. & Sayanna, R. Optical properties of bismuth borate glasses doped with Eu³⁺ ions. *Int. Conf. Condens. Matter Appl. Phys.* **1728**, 020377 (2016).
59. Ahmad, F., Aly, E. H., Atef, M. & ElOkr, M. Study the influence of zinc oxide addition on cobalt doped alkaline earth borate glasses. *J. Alloy. Compd.* **593**, 250–255 (2014).
60. Nazrin, S. N. *et al.* Dielectric constant, metallization criterion and optical properties of CuO doped TeO₂-B₂O₃ glasses. *J. Inorg. Organomet. Polym. Mater.* **32**(7), 2513–2526 (2022).
61. Ghazy, A. R. *et al.* Synthesis, structural and optical properties of Fungal biosynthesized Cu₂O nanoparticles doped Poly methyl methacrylate-co-Acrylonitrile copolymer nanocomposite films using experimental data and TD-DFT/DMO₃ computations. *J. Mol. Struct.* **1269**, 133776 (2022).
62. Ghazy, A. R., Al-Hossainy, A. F., Rizk, H. F. & Shendy, S. Synthesis, characterization, TD-DFT method, and optical properties of novel nanofiber conjugated polymer. *Synth. Met.* **291**, 117206 (2022).
63. ElBatal, F., Hamdy, Y. & Marzouk, S. UV-visible and infrared absorption spectra of transition metals-doped lead phosphate glasses and the effect of gamma irradiation. *J. Non-Cryst. Solids* **355**, 2439–2447 (2009).
64. Mercier, C., Palavit, G., Montagne, L. & Follet-Houttemane, C. A survey of transition-metal-containing phosphate glasses. *C. R. Chim.* **5**, 693–703 (2002).
65. Haddon, J., Rogers, E. & Williams, D. Absorption spectra of first row transition metal ions in phosphate glasses. *J. Am. Ceram. Soc.* **52**, 52–52 (1969).
66. ElBatal, F., Marzouk, M. & Abdelghany, A. UV-visible and infrared absorption spectra of gamma irradiated V₂O₅-doped in sodium phosphate, lead phosphate, zinc phosphate glasses: A comparative study. *J. Non-Cryst. Solids* **357**, 1027–1036 (2011).
67. El Agammy, E., Doweidar, H., El-Egili, K. & Ramadan, R. Physical and optical properties of NaF-TeO₂ glasses and glass-ceramics. *Appl. Phys. A* **127**, 1–9 (2021).
68. Gautam, S., Bundela, P., Pandey, A., Awasthi, M. & Sarsaiya, S. Diversity of cellulolytic microbes and the biodegradation of municipal solid waste by a potential strain. *Int. J. Microbiol.* <https://doi.org/10.1155/2012/325907> (2012).
69. Tauc, J., Grigorovici, R. & Vancu, A. Optical properties and electronic structure of amorphous germanium. *Phys. Status solidi (b)* **15**, 627–637 (1966).
70. Ghazy, A., Hemeda, O., Al-Hossainy, A., Ghazy, R. & Henaish, A. Docking of COVID-19 main protease and TD-DFT/DMO₃ simulated method, synthesis, and characterization with hybrid nanocomposite thin films and its applications. *Surf. Interfaces* **37**, 102722 (2023).
71. Larsson, P. *et al.* Optimization of cell viability assays to improve replicability and reproducibility of cancer drug sensitivity screens. *Sci. Rep.* **10**, 1–12 (2020).
72. Chen, S. *et al.* In vitro stimulation of vascular endothelial growth factor by borate-based glass fibers under dynamic flow conditions. *Mater. Sci. Eng., C* **73**, 447–455 (2017).
73. Palakurthy, S., Reddy, K. V., Patel, S. & Azeem, P. A. A cost effective SiO₂-CaO-Na₂O bio-glass derived from bio-waste resources for biomedical applications. *Prog. Biomater.* **9**, 239–248 (2020).
74. Moghanian, A. *et al.* Structural and in vitro biological evaluation of sol-gel derived multifunctional Ti⁴⁺/Sr²⁺ co-doped bioactive glass with enhanced properties for bone healing. *Ceram. Int.* **47**, 29451–29462 (2021).
75. Datta, S. *et al.* Effect of boron oxide addition on structural, thermal, in vitro bioactivity and antibacterial properties of bioactive glasses in the base S53P4 composition. *J. Non-Cryst. Solids* **498**, 204–215 (2018).
76. Balasubramanian, P., Buettner, T., Pacheco, V. M. & Boccaccini, A. R. Boron-containing bioactive glasses in bone and soft tissue engineering. *J. Eur. Ceram. Soc.* **38**, 855–869 (2018).

Author contributions

A.R.G.: Conceptualization, Methodology, Formal analysis, Investigation, Writing—Review & Editing; B.M.E.: Conceptualization, Formal analysis, Investigation, Writing; A. M.A.: Conceptualization, Formal analysis, Investigation, Writing, reviewing final version; T.M.M.: Conceptualization, Methodology, Writing—Original Draft, Writing—Review & Editing; R.G.: Conceptualization, Methodology, Formal analysis, Investigation, Writing—Review & Editing; R.M.R.: Supervision, Conceptualization, Methodology, Writing—Original Draft, Writing—Review & Editing.

Funding

Open access funding provided by The Science, Technology & Innovation Funding Authority (STDF) in cooperation with The Egyptian Knowledge Bank (EKB).

Competing interests

The authors declare no competing interests.

Additional information

Correspondence and requests for materials should be addressed to A.R.G.

Reprints and permissions information is available at www.nature.com/reprints.

Publisher's note Springer Nature remains neutral with regard to jurisdictional claims in published maps and institutional affiliations.



Open Access This article is licensed under a Creative Commons Attribution 4.0 International License, which permits use, sharing, adaptation, distribution and reproduction in any medium or format, as long as you give appropriate credit to the original author(s) and the source, provide a link to the Creative Commons licence, and indicate if changes were made. The images or other third party material in this article are included in the article's Creative Commons licence, unless indicated otherwise in a credit line to the material. If material is not included in the article's Creative Commons licence and your intended use is not permitted by statutory regulation or exceeds the permitted use, you will need to obtain permission directly from the copyright holder. To view a copy of this licence, visit <http://creativecommons.org/licenses/by/4.0/>.

© The Author(s) 2023